Journal of Volcanology and Geothermal Research 183 (2009) 84–96

Contents lists available at ScienceDirect

Journal of Volcanology and Geothermal Research

journal homepage: www.elsevier.com/locate/jvolgeores

Hydromagmatic eruption during the buildup of a Triassic carbonate platform (Oman Exotics): Eruptive style and associated deformations

Christophe Basile *, François Chauvet [1]

Laboratoire de Géodynamique des Chaînes Alpines, CNRS UMR 5025, Observatoire des Sciences de l'Univers de Grenoble, Université Joseph Fourier, Maison des Géosciences, 1381 rue de la Piscine, 38400 St Martin d'Hères, France

ARTICLE INFO

Article history:
Received 20 October 2008
Accepted 11 March 2009
Available online 26 March 2009

Keywords:
phreatomagmatic eruption
sill
magma stock
megabreccia
carbonate platform
diatreme

ABSTRACT

Oman Exotics represent remnants of a Triassic carbonate platform, also named Misfah Formation. Several basaltic intrusions or lava flows were coeval with the carbonate platform buildup. We present field observations related to one of these volcanic events, including associated deformation of the host rocks and interaction of volcanism with the sedimentation. These observations allow us to reconstruct the structure of the volcanic conduit and vent and the successive stages of the evolution of the eruption. The initial ascent of magma probably occurred along on a normal fault related to gravity-driven sliding towards the platform edge. Magma was first emplaced in a saucer-shaped sill a few tens of meters below the sea-floor. This intrusion provided a decollement layer, that may have sped up the gravity-driven sliding, opening fractures that brought sea water into contact with the magma, hence triggering a hydromagmatic eruption. Eruption was followed by the collapse of the host limestones that formed a megabreccia infilling the eruptive vent and prohibiting further contact between sea water and magma. Most of the magma was emplaced at depth in two superposed small magmatic bodies (300×100 m and 200×50 m in sections, respectively) that replaced the host sediments and uplifted the overlying vent. Despite the shallow submarine setting, this eruption produced a vent quite similar to sub-aerial maars developed in soft substrate. This emphasizes that the rheology of the substrate may be more important than the amount of water to control magma–water interaction in hydromagmatic eruptions. In an active carbonate platform like Misfah Formation during Triassic times, the early diagenesis of lime mud determined the mechanical comportment of the sediment at the time of eruption, and especially the way it could be mixed with the magma and/or slide into the vent.

1. Introduction

Since the birth of Surtsey (Thorarinsson, 1967; Kokelaar, 1983) and Capelinhos (Machado et al., 1962; Cole et al., 2001) volcanic islands, the interaction of magma and external water appeared as one of the most important factors influencing the volcanic eruption processes (Sheridan and Wohletz, 1983; Zimanowski et al., 1991). This interaction results from an efficient heat transfer from the magma to the water, generating large amounts of steam. When lava and water come together in an underground closed space, the increasing volume of steam may induce overpressure, triggering an explosive reaction and hydromagmatic eruption. The morphology, structure and lithology of the volcanic edifices built by hydromagmatic eruptions vary with the ratio of magma interacting with water (Sheridan and Wohletz, 1983) or water-rich sediments (White, 1996), and with the local conditions that bring magma and water into contact. Many examples of hydromagmatic eruptions have been described all over the world, and over various types of substratum. The two main types are:

(1) Sub-aerial maars (e.g. Lorenz, 1974), where magma encounters ground or underground water. The evolution of this type of volcano depends on the rheology of the substratum (soft- and hard-substrate maars: Lorenz, 2003; Sohn and Park, 2005; Martin and Nemeth, 2005; Auer et al., 2007), and on the way water and magma circulate to produce a series of explosions within the diatreme (Lorenz and Kurszlaukis, 2007).
(2) Shallow-marine Surstey-type eruptions (e.g. Kokelaar, 1983), where magma enters within a large volume of surface water. The interaction of magma with water in excess produces numerous explosions that build tuff cones and/or rings by fallout and pyroclastic surges (Cole et al., 2001; Solgevik et al., 2007).

Carbonate platforms represent a large proportion of shallow-marine environments, but we found only a few published observations of volcanic eruptions during carbonate platform buildup. In most cases, carbonate platforms developed above or on the side of inactive volcanoes, either in intraplate settings (e.g. Hess, 1946; Matthews et al., 1974), or in subduction-related volcanic arcs (e.g. Fulthorpe and

* Corresponding author. Tel.: +33 4 765 140 69; fax: +33 4 765 140 58.
E-mail addresses: cbasile@ujf-grenoble.fr (C. Basile), francois.chauvet@univ-nantes.fr (F. Chauvet).
[1] Present address: Laboratoire de Planétologie et Géodynamique de Nantes, CNRS UMR 6112, Université des Sciences de Nantes, 2 rue de la Houssinière, BP92208, 44322 Nantes Cedex 3, France.

0377-0273/$ – see front matter © 2009 Elsevier B.V. All rights reserved.
doi:10.1016/j.jvolgeores.2009.03.009

Schlanger, 1989; Soja, 1996). When volcanism and carbonate platform sedimentation are coeval, they are mainly restricted to interstratification of sediments and lava flows or volcanic fallouts (e.g. Buigues et al., 1992; Soja, 1996; Beltramo, 2003).

We found only a few examples of volcanism contemporaneous with a growing carbonate platform, such as the Triassic dikes and lavas emplaced in the Dolomites (Southern Alps: Blendinger, 1985), or an Albian basaltic intrusion and associated volcaniclastic sediments in Spain (Fernández-Mendiola and García-Mondéjar, 2003). Actually, the best described example of shallow-marine eruption through a growing carbonate platform is the MIT guyot in the Pacific ocean (Shipboard Scientific Party, 1993; Martin et al., 2004). There, a 200 m-thick tephra unit is interpreted as resulting from a submarine eruption through a semi-solidified early Aptian carbonate platform. Tephra consists of palagonitized basaltic clasts, carbonate mud- to grainstone clasts and armoured lapilli (Martin et al., 2004). They were emplaced by mass flows and gravity-driven sliding inside the volcanic vent. However, this study based on drilling cores does not provide information at the vent scale nor for the successive stages of the eruption.

In this paper, we describe the interaction of a volcanic eruption with the formation of a Triassic carbonate platform in Oman. Since a full section of this volcanic edifice outcrops, it provides outstanding observations of the geometry of the vent, of the successive stages of the eruption, and allows one for the first time to evaluate the respective evolutions of the feeding system, water–magma contact zone and subsea volcanic edifice, emphasizing associated small- and large-scale deformations.

2. Geological setting

As part of the southern margin of the Neo-Tethys ocean, the Oman continental margin formed during Permian–Triassic times (Béchennec, 1988; Robertson and Searle, 1990; Sengör et al., 1993). Palinspatic reconstructions suggest the development of contrasted sedimentary environments since Middle Permian times, with a continental platform (Saiq Formation: Glennie et al., 1974), a continental slope (Sumeini Formation: Glennie et al., 1974), and basinal environments (Hawasina Formations: Glennie et al., 1974; Béchennec, 1988). Sumeini and Hawasina formations were thrusted on the Arabian platform during the upper Cretaceous obduction of the Sumail ophiolites (Béchennec et al., 1988) (Fig. 1). It is noteworthy that the paleopositions of the sedimentary units on the continental margin were mainly derived from their positions in the tectonic pile, assuming an outward thrust sequence (Glennie et al., 1973, 1974; Béchennec, 1988; Robertson and Searle, 1990). There is an ongoing debate on the nature of the basement below the Hawasina basin, supposed to be either oceanic (Glennie et al., 1973, 1974; Stampfli et al., 1991; Pillevuit et al., 1997), continental (Béchennec, 1988; Béchennec et al., 1990, 1991) or intermediate (Graham, 1980; Searle and Graham, 1982). As a consequence, the Permian (e.g. Pillevuit et al., 1997) or Triassic (e.g. Béchennec, 1988) age for the onset of the oceanic accretion is also a matter of debate.

During Triassic times, a carbonate platform developed within the Hawasina basin. Because they are mainly found in tectonic slices, remnants of this platform were named Oman Exotics by Glennie et al. (1974). They were referred to the Kwar Group by Béchennec (1988). In the Hawasina nappes, the Kwar Group crops out mainly south of the western termination of Jabal Akhdar anticline in several mountains dominated by high carbonate cliffs: Jabal Misht, Jabal Misfah, Jabal Kwar, and Jabal Ghul (Fig. 1). This Group has been divided by Béchennec (1988) into four Formations, later-on subdivided into six Formations by Pillevuit (1993). Stratigraphy has been defined on the northern and eastern slopes of Jabal Misfah (Fig. 2).

(i) At the base, a volcanic unit is composed of massive basaltic pillow lavas, hyaloclastites and fine-grained volcanogenic sediments (tuffites), and dated Ladinian–Carnian from foraminifera found in few intercalated limestones (Pillevuit, 1993). This unit thrusts the Late Permian to Liasic bathyal sedimentary rocks of Al Jil (limestones and cherts) and Matbat (limestones, sandstones and siltstones) Formations (Beurrier et al., 1986).

(ii) Above the volcanic unit, the Misfah Formation is made of thinly bedded marly limestones at the base (Subayb Formation,

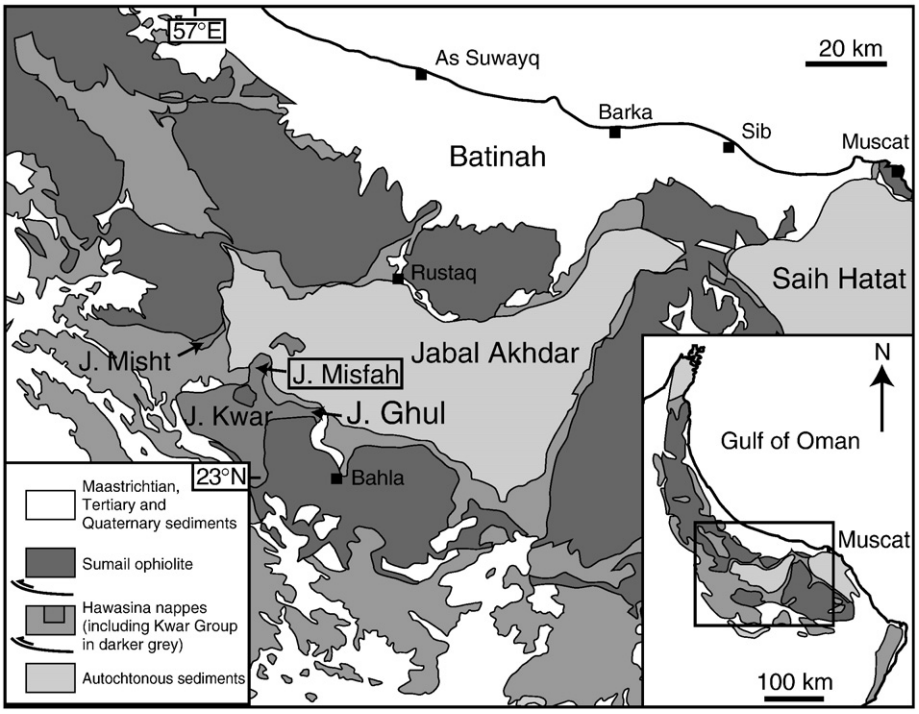

Fig. 1. Location of the studied area (Jabal Misfah, boxed) in a simplified geological map of central and eastern Oman Mountains (modified after Béchennec et al., 1990). Inset: simplified geological map of northern Oman, modified after Glennie et al., 1974.

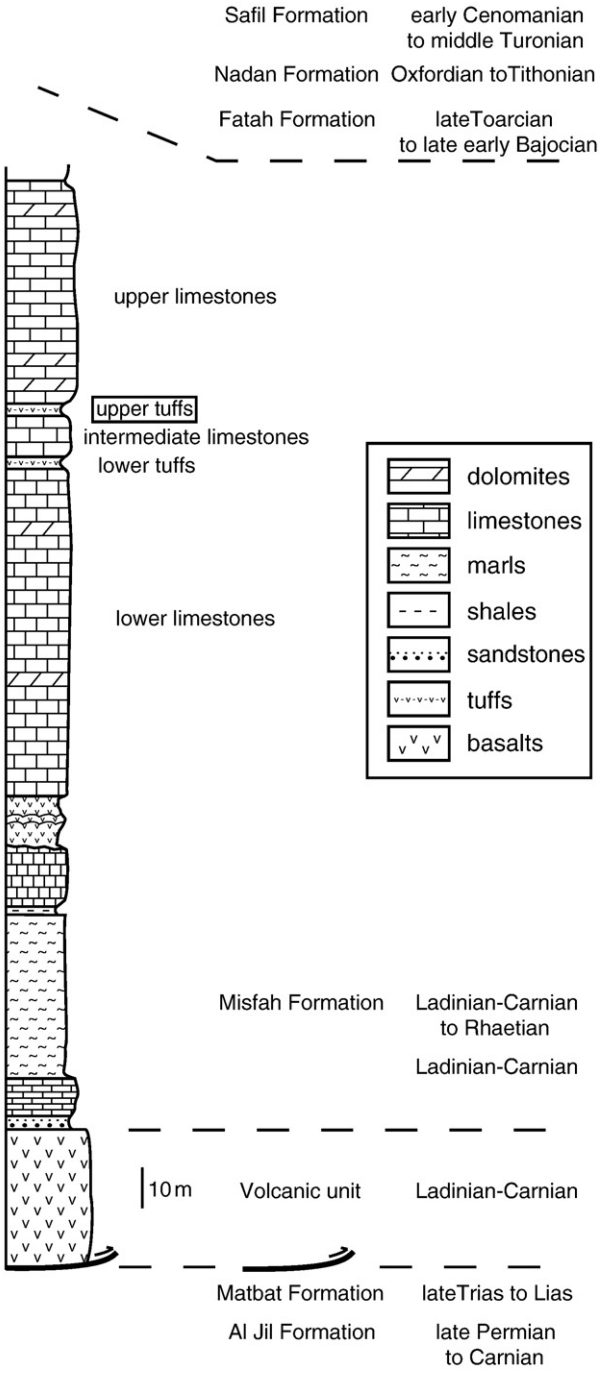

Fig. 2. Stratigraphy of the Kwar Group. Lithologic log is detailed only in the lowest part of Misfah Formation (see text for details). Ages according to Pillevuit et al. (1997) and Beurrier et al. (1986). The studied magmatic event is related to the upper tuffs (boxed).

Pillevuit, 1993), overlain by thick and massive platform limestones. These two members were dated respectively Ladinian–Carnian, and Ladinian–Carnian to Rhaetian by Pillevuit (1993). Krystyn (in Baud et al., 2001) proposed a revised age of Middle–Late Norian for the lower member, and topmost Norian–Rhaetien for the upper member. Few intercalations of coarse- to fine-grained volcaniclastic sediments occur in the lower part of Misfah Formation, also intruded by basaltic dikes and sills.

(iii) The upper part of the Kwar group consists of pelagic limestones from the Jurassic to Cretaceous Fatah (Pillevuit, 1993), Nadan and Safil Formations.

3. Field observations

3.1. Stratigraphy

The studied volcano-sedimentary section belongs to the lowest part of the Misfah Formation, northeast of Jabal Misfah, near Subayb hamlet. It may belong to the Subayb Formation as defined by Pillevuit (1993), but we do not support this stratigraphic terminology as both published reference sections appeared to be limited upward by tectonic contacts. The description of volcanic and sedimentary section here (Fig. 2) synthesizes observations from the northeastern part of Jabal Misfah, omitting the numerous and more recent magmatic intrusives and fault offsets. It is important to note that while carbonates are laterally extensive, effusive and intrusive magmatic formations occur only locally.

Above submarine basaltic volcanic rocks (pillow lavas and hyaloclastites), the sedimentary section begins with a few beds of volcanic pebbles in a carbonate matrix. Then a first carbonate unit comprises from the base to the top 10 m of decimeter-thick beds of yellow marly limestones, 40 m of wavy-bedded marly limestones, 2 m of marls, and 15 m of thirty centimeters-thick grey limestones strata (Fig. 2). These carbonates are locally truncated by a twelve meter-thick volcano-sedimentary unit including, from base to top, tuffites, volcanic breccia, submarine lava flows and elongated globular volcanic clasts mixed with sediments. Directly above begins a second carbonate unit, approximately one hundred and fifty meters-thick, made of thirty centimeter-thick beds of black limestones with a few white stromatolithic layers. Two meter- to a few meters-thick volcano-sedimentary layers are intercalated within this carbonate unit. They consist mainly of tuffites, with volcanic and sedimentary clasts, separated by a few limestone beds exhibiting numerous sliding structures. According to Pillevuit (1993), this second carbonate unit was deposited at shallow depths, mainly in the tidal zone. In the following description of the studied magmatic event, the various parts of this second carbonate unit are referred to as (from base to top) lower limestones, lower tuffs, intermediate limestones, upper tuffs, and upper limestones (Fig. 2).

3.2. Magmatic event

3.2.1. Vent and ejecta

The stratigraphic units appear continuously along Jabal Misfah cliffs. However, important variations occur in a 500 meters-wide area southwest of Subayb hamlet (Figs. 3A and 4). Here the upper tuffs do not lie as usual on intermediate limestones, but on a megabreccia lying itself on an erosional surface cutting the intermediate limestones, the lower tuffs and the lower limestones (Fig. 4). The megabreccia consists of meter- to decameter-scale limestones beds tilted in an intraformational breccia composed of angular blocks of the eroded limestones mixed in a grey limestone matrix (Fig. 5). It is noteworthy that some basaltic gravels occur within the limestone breccia, but that there is no volcanic nor volcano-detritic layer between the megabreccia and the erosional surface. The megabreccia is laterally continuous with the intermediate limestones, where numerous tension gashes develop. These tension gashes are connected to and filled by interlayed marly limestones, suggesting in situ brecciation. The megabreccia and its tilted blocks are sealed by few meters of platy limestones, then by the upper tuffs, thickening up to 15 m (Fig. 4). In this area, the upper tuffs consist of intercalations of thin tuffite beds with massive breccia made of limestones and a few basaltic blocks in a calcareous matrix. In the overlying upper carbonates, there are no lateral variations of facies nor thicknesses.

Below the megabreccia, the erosional surface deepens toward a central point where there are no more lower limestones, but a mix of basalt and sediments, overlying massive basalts (Fig. 4). The erosional surface affects a 150 meter-wide zone southwest of this

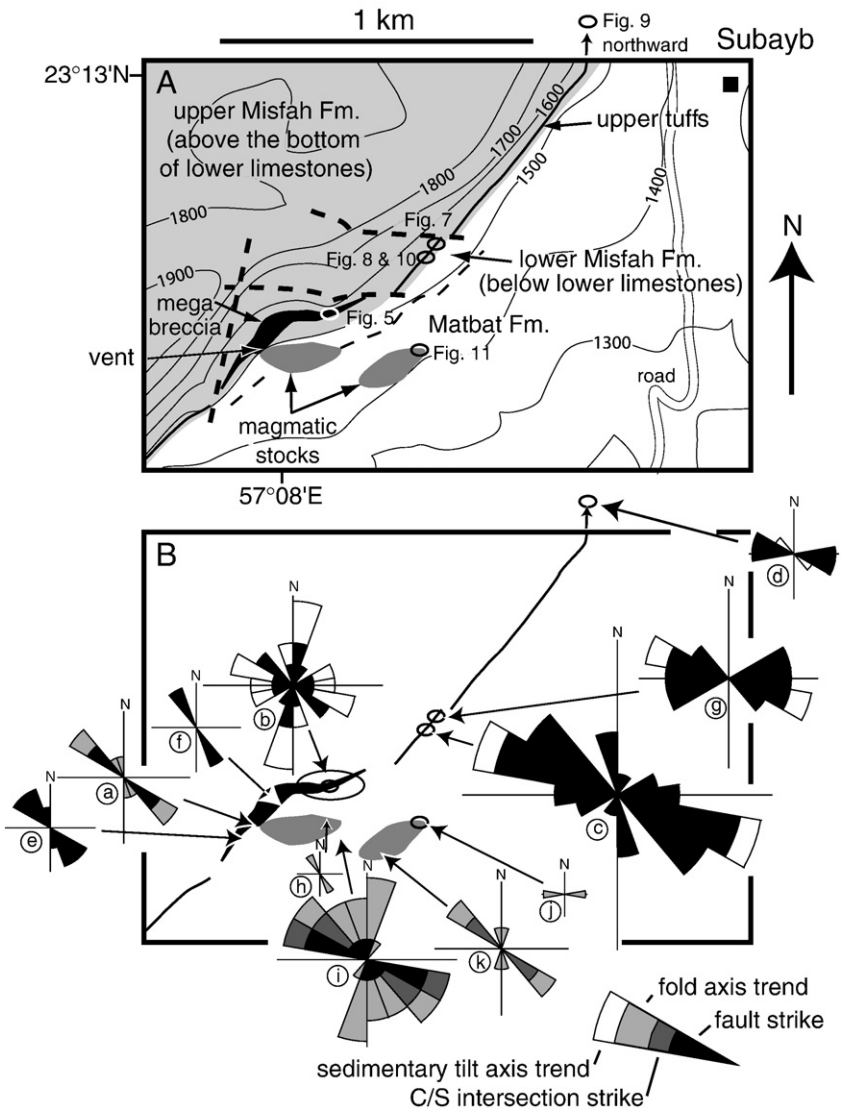

Fig. 3. (A) Schematic geological map of the studied area. Topography (meters) from Beurrier et al., 1986. Thick stippled lines are recent faults, thin stippled line represents the unobserved limit between Misfah and Matbat formations. Figs. 5, 7 to 11 are located by ellipses. (B) Same as in panel A, with location of the upper tuffs, megabreccia and magmatic stocks, and rose diagrams of structural observations. Rose diagrams (a) to (k), see comments in the text. Same scale for all rose diagrams, maximum seven values on rose c. All structural measurements are related to the same magmatic event, with the exception of N–S structures at sites (i) and (k) which are related to a more recent eastward normal shear.

central point, and a wider (300 m) zone northeastward, where erosion reaches deeper levels (Fig. 4).

The upper tuffs contain numerous lapilli in a cryptocrystalline lime mud matrix (Fig. 6), where glassy or palagonitized shards are commonly observed. Most lapilli cores are calcareous, although others are derived from volcanic lithic fragments or glass. The edges of lapilli cores are very irregular, corroded and underlined by oxidation (Fig. 6D). Lapilli rims also include palagonitized

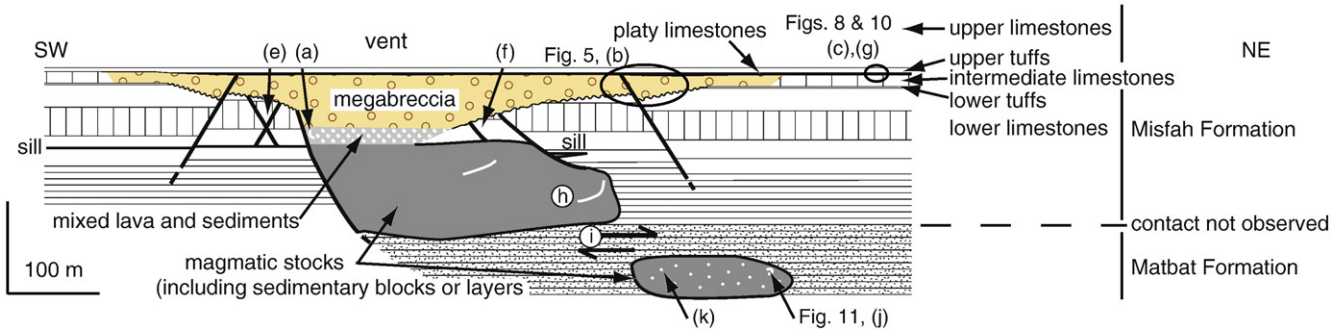

Fig. 4. Section across the eruptive point, reconstructed at the time of deposition of the upper limestones. Figs. 5, 8, 10 and 11, and rose diagrams (a) to (k) (Fig. 3) are located by ellipses or arrows. White dots and lines in the magmatic stocks represent sedimentary blocks and layers, respectively.

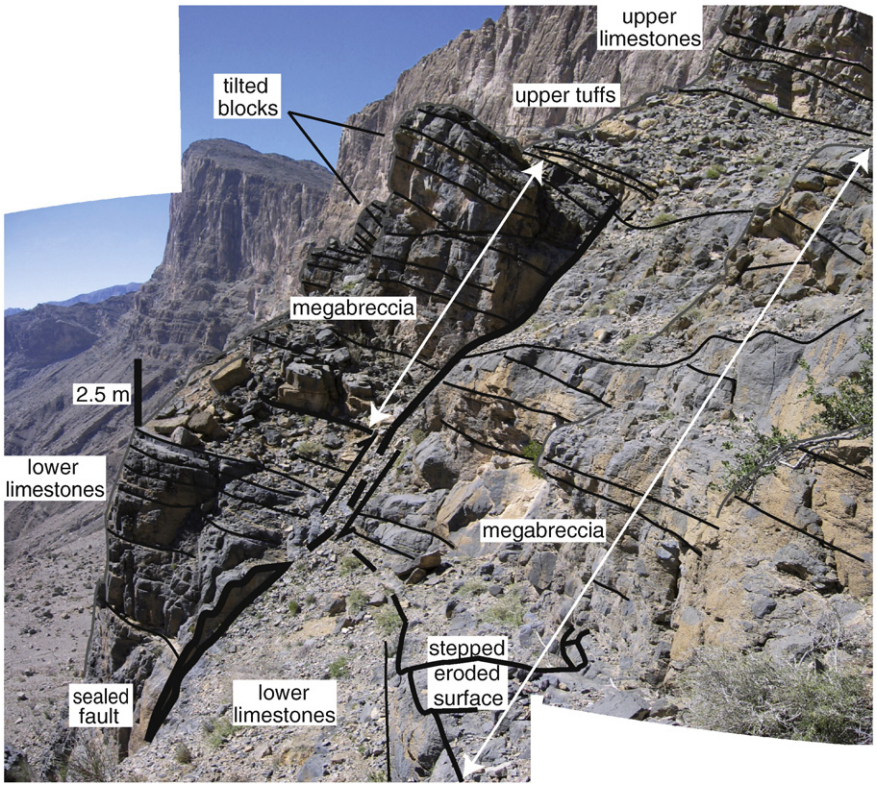

Fig. 5. View towards southwest of the megabreccia. Indicative scale (beware the perspective). Note the tilted blocks within the megabreccia, its stepped and erosive basal surface, and the normal fault sealed by the upper tuffs. The upper part of Misfah Formation forms the cliffs in the background. Structural observations made in this area are shown in Fig. 3B in the rose diagram (b). Location Figs. 3 and 4.

shards in a cryptocrystalline matrix showing concentric structures (Fig. 6).

At the base of the upper tuffs, numerous shells are reworked from an underlying lumachelle, and mixed with limestone clasts in the tuff matrix. This indicates that the substratum of the upper tuffs has been locally eroded at the time of tuff emplacement, and that the products of erosion were mixed with the tuffs in their lowermost part. Above, thinly layered tuffs exhibit basaltic and limestone clasts, as big as 1 m in diameter. The asymmetric impact sags (Fisher, 1977) show that the blocks were ejected from the southwest and fell on previously deposited tuffs (Fig. 7). The same displacement of ejecta towards N10° is indicated by oblique bedding in small (twenty centimeters-high) dunes (Fig. 8).

We interpret this erosional zone as a volcanic vent (White, 1991; Lorenz, 2003). The infilling megabreccia resulted from the collapse of its walls, and the upper tuffs represent the ejecta deposited during the eruption.

3.2.2. Faulting in the host limestones

During the magmatic event, some normal faults affected the underlying limestones (Fig. 4). These faults were all sealed by the upper tuffs. At the top of the massive basalts, the southwest edge of the vent is a normal fault striking N130°, that separates the lowest part of the lower limestones from the base of the megabreccia (Figs. 3B-a and 4). Some conjugated normal faults striking N155° occur on both sides of the vent (Fig. 3B-e and f). They were all sealed by the megabreccia. Northward the significant throws are located on north-dipping normal faults, while southward the southernmost fault dips south. Those faults farther from the center of the vent shift the erosive base of the megabreccia (Figs. 4 and 5), indicating they were slightly younger than the conjugated faults closer to the center of the vent. These younger normal faults define a small horst centered on the eruptive point. It is noteworthy that the strike of the normal faults significantly changes from N160° southwestward to N110° northeastward, while the NNE–SSW stretching direction indicated by the deformation of the upper tuff layers does not significantly change (Fig. 3B-a to g).

In the megabreccia, as in the in situ brecciated intermediate limestones, numerous sliding structures were observed. The sliding blocks consist at least partly of dolomite beds, probably more lithified than the limestones at the time of the sliding. Sliding planes and syn-sedimentary tilt axes in the megabreccia and intermediate limestones predominantly strike either N110° or N–S (Figs. 3B-b to d and 9). They are sliding towards the center of the vent, with the exception of a structure observed as far as 1.8 km northeastward (Figs. 3B-d and 9). Similarly, we observed several syn-sedimentary listric faults in the platy limestones, indicating NNE–SSW extension and sliding towards the center of the vent (Figs. 3B-c and 10).

3.2.3. Intrusions

Within the vent, folded beds of limestones are mixed together with a basaltic breccia containing numerous calcareous clasts and blocks. Folds are roughly cylindrical, with sub-horizontal axial surfaces and axes trending N130° to N150° (Fig. 3B-a). Right below the eruptive point, scree hides the deep structures, which can only be seen northward below the lower limestones. There, a basaltic body intrudes the wavy-bedded limestones (Figs. 3A and 4). In this magmatic body, blocks or beds of the enclosing or overlying limestones are mixed with basalts. Some limestone beds are longer than 40 m, and folded with a N150°-trending axis (Fig. 3B-h). The enclosing limestones are cross-cut by N130°-trending dikes, and locally by a sill connected with the main magmatic body, that pinches out laterally and accommodates the incipient fall of a limestone block at the side of the magmatic body (Fig. 4). We made no observation indicating that the magma may have pushed away the host rock laterally. Upward push is probable, but would have been very restricted when compared with the thickness of the magmatic body. It seems that the magmatic body was emplaced

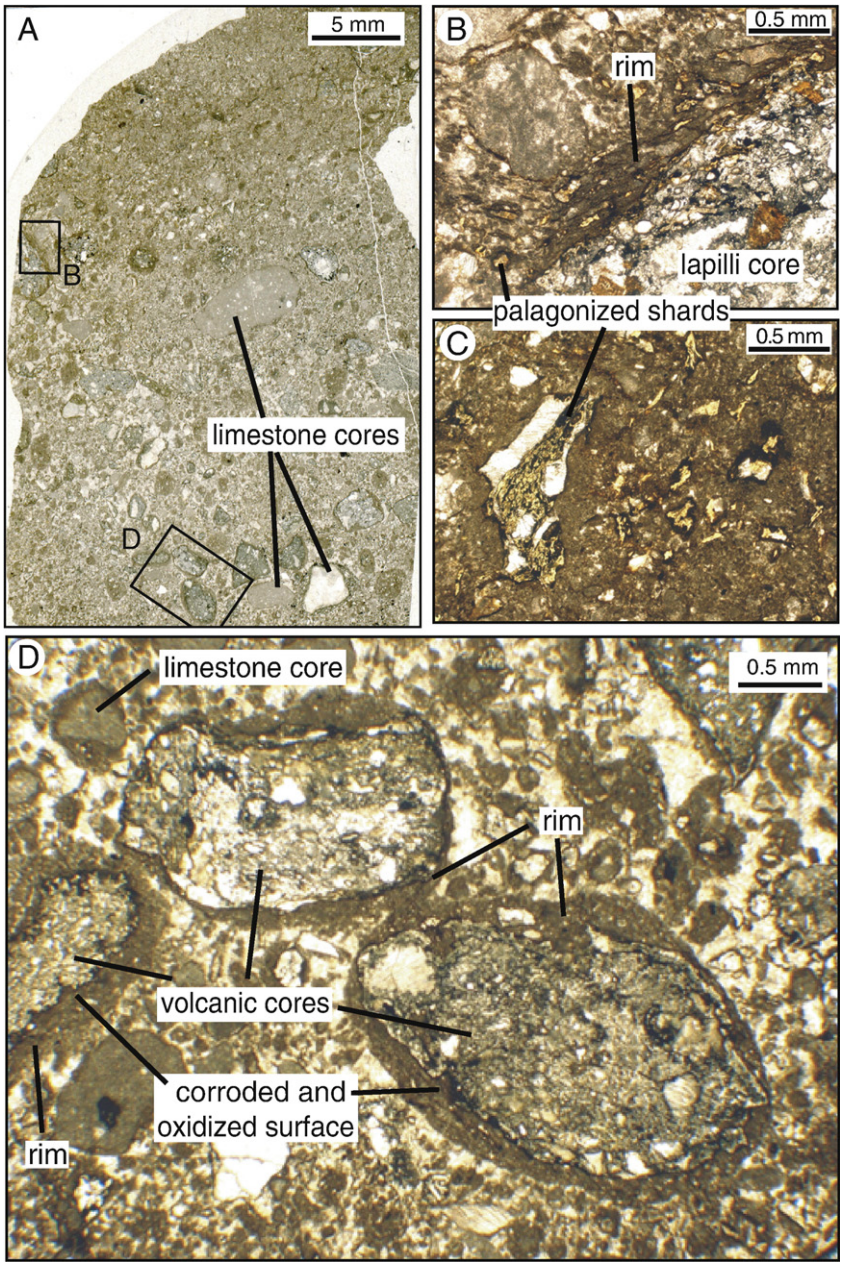

Fig. 6. Texture of the upper tuffs. A: scanned thin section. B: lapilli rim with yellowish glassy shards in a cryptocristalline matrix. C: glassy shards palagonized and oxidized in the tuffs matrix. D: armoured lapillis with altered volcanic cores. Note the corroded edges of the volcanic fragments. Panels B and D are located in panel A; Panel C is a detail from another thin section.

by fracturing the host rock and assimilating at least partially the limestone blocks.

The basalts are quite homogeneous in the magmatic body, with the exception of an increasing alteration upward. Alteration probably results from higher water content at the time of the magmatic event. No trace of a magmatic body has been found south of the eruptive point, but a basaltic sill underlines the base of the lower limestones (Fig. 4). While presently horizontal, this sill is offset by a normal fault sealed by the upper tuffs.

Below the magmatic body, several tens of meters of pelagic silicified limestones and sandstones attributed to the Matbat Formation were deformed by two successive ductile events: normal shearing towards N50° characterized the older one; N–S trending folds represent a younger eastward normal shear (Fig. 3B-i). There is no significant shear zone between the Matbat limestones and the overlying basalts, but both are interlayered and affected by the two ductile deformations, suggesting that the magma was ductile at the time of deformation. Below these deformed sediments, similar limestone beds and blocks from the Matbat Formation are included inside a deeper magmatic body, where radiolarites were also found as xenoliths. As in the upper magmatic body, sedimentary beds are often folded, with fold axes trending N90° to N140° (Figs. 3B-j and 11). Shear zones indicate top-to-N50° displacements (Fig. 3B-k). The sedimentary blocks or layers are clearly metamorphosed in this lower magmatic body, while they are not, at macroscopic scale, in the upper stock.

4. Interpretation

4.1. Structure

The vent and both upper and lower magmatic bodies appear aligned in a WNW–ESE direction parallel to the main normal faults

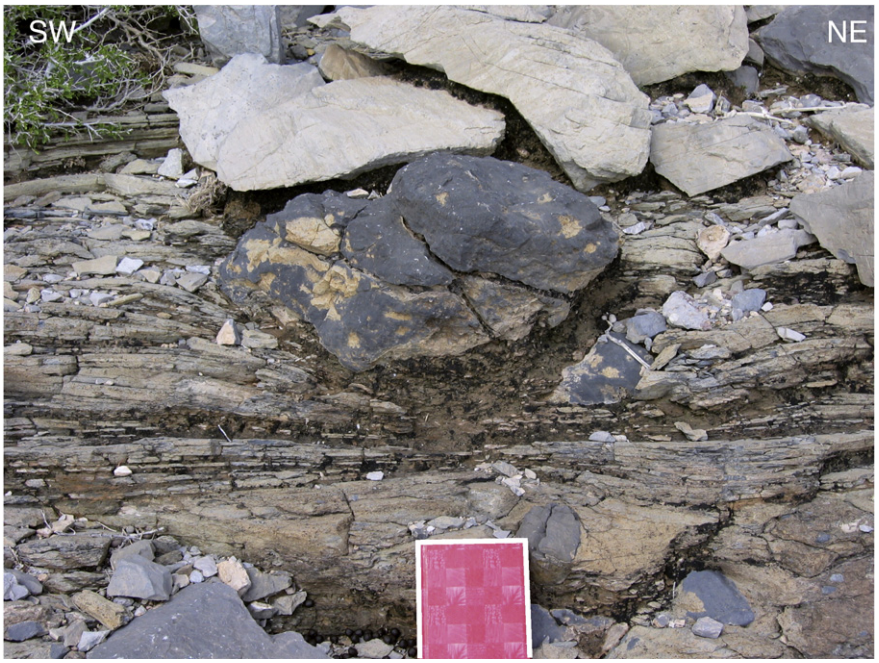

Fig. 7. Ballistically-emplaced limestone block. The grey limestone blocks were projected in the tuffs. The white limestones blocks are screes from the above cliff. Notebook for scale (17.5 cm-high, 11.5 cm-wide). Structural observations made around this outcrop are shown Fig. 3B in rose diagram (g). Location Fig. 3.

(Fig. 3B). This feature cannot be fitted by a circular crater, i.e. a structure centered on the eruptive point. As this linear disposition is parallel or sub-parallel with the normal fault bounding the eruptive point, with the other major normal faults, and with the shear zones at depth, it suggests that both magmatic and tectonic processes were associated in a NE–SW extensional tectonic regime, and that the magma probably rose to the subsurface along a WNW–ESE-trending fissure.

We also observed slight changes in the strike of the main normal faults, from N160° in the southwestern part of the outcrop, to N110° eastwards or northeastwards (Fig. 3B). Moreover, N110°-striking normal faults are in some places associated with N–S-striking normal faults or sliding structures (Fig. 3B-b and c). These N110° and N–S structures may have been formed as conjugated faults in a transtensional regime, indicating a N60° lengthening direction, perpendicular to N160° normal faults. Both changes in orientation and transtension can be explained by a homogeneous displacement on an arcuate structure (Fig. 12): in the central part, displacement is perpendicular to the structure, and results in N110°-striking normal faults in an extensional regime; on the sides, displacement becomes oblique, and can be partitioned in divergence perpendicular to the structure, and strike-slip parallel to the structure. The resulting faults are either controlled by the transtensional tectonic regime (conjugated N110°- and N–S-striking faults), or by the local topography imposed by the main structure (N160°-striking normal faults, parallel to the main structure). As subsurface deformation is probably linked to the magma-feeding fissure, this interpretation

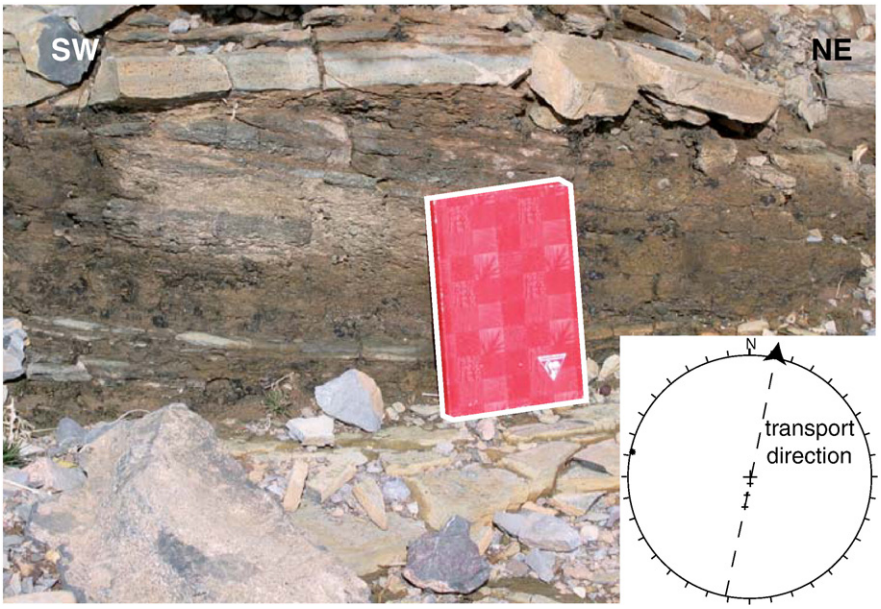

Fig. 8. Dune structure in the upper tuffs. Same notebook as for Fig. 7. Wulff net (lower hemisphere): small crosses are poles for bedding, stippled great circle and star are the best great circle for bedding and its pole (i.e. the axis of rotation), respectively. Location Figs. 3 and 4.

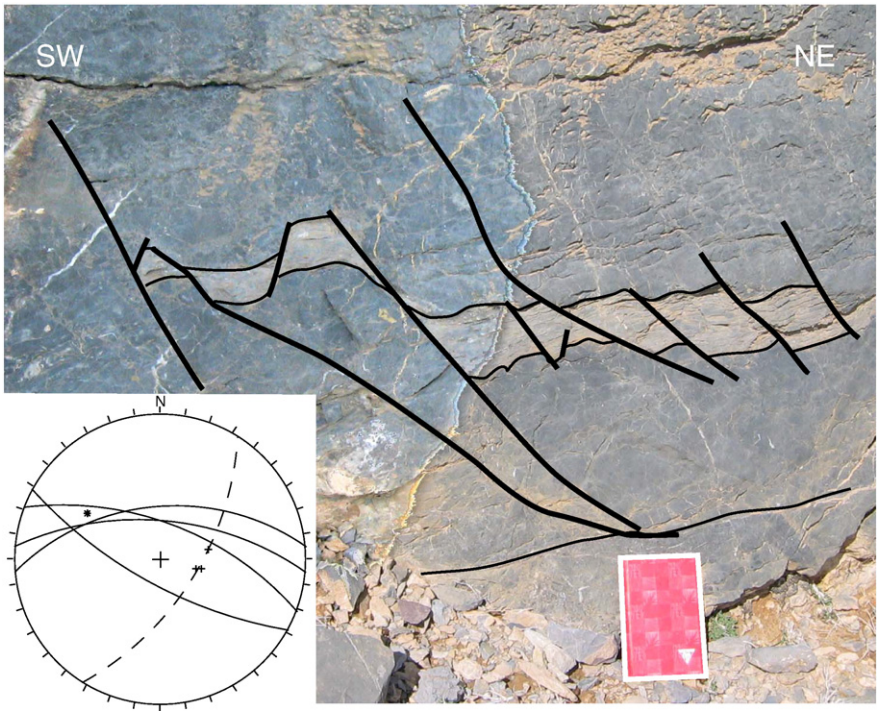

Fig. 9. Syn-diagenetic normal faults in the intermediate limestones, indicating sliding towards N30°. Same notebook as for Fig. 7. Same legend as for Fig. 8 for the stereo net. Great circles are normal faults. Structural measurements are also shown Fig. 3B in rose diagram (d). Approximate location Fig. 3.

suggests that the feeding fissure may be curved and several kilometers-long.

Moreover, several observations indicate an asymmetry in the deformation: the lower limestones are more thinned and the normal faults more numerous north of the vent than southward, the main normal faults are dipping northeast as the fault bounding the vent, the deep shear zones also indicate displacements toward NE. This suggests that the carbonate platform was stable southwest of the feeding fissure, while the northeastern part slid northeastward on the intrusive magma and a deep shear zone, possibly towards the edge of the carbonate platform.

4.2. Hydromagmatic eruption

In the upper tuffs, the volcanic shards are palagonitized, and the surfaces of volcanic cores in lapilli are commonly corroded and oxidized (Fig. 6). This suggests that these tuffs resulted from an explosive mixing of magma and steam, where volcanic shards were hydrated and corroded. Together with other ejected objects as spinel crystals or sedimentary fragments, they were wrapped within the eruption cloud by a rim of heated mud, and fallout to form the upper tuffs. All these elements favour hydromagmatic processes, where the eruption results from the production of over-pressured steam by underground mixing of water and magma (Wohletz, 1986; White, 1996).

Several observations indicate that the tuff layer is related to a subaerial eruption. These observations include well-bedded and locally dune-bedded poorly sorted sediments (Fig. 8) (e.g. Gençalioglu-Kuscu et al., 2007; Pardo et al., 2008), isolated cobbles and boulders of limestones associated with impact sags (Fig. 7) (Fisher, 1977; Pardo et al., 1998), and base surge (Fisher, 1977) suggested by in situ erosion and resedimentation of shells at the base of the tuffs.

Finally, it is obvious from its location that this phreatomagmatic eruption occurred within a carbonate platform. Moreover, the lime mud nature of the tuff matrix, the numerous limestone clasts in the tuffs, the limestone boulders associated with impact sags, and the mechanical behavior of the megabreccia point out the variable diagenesis in the host limestones at the time of eruption: while limestone and dolomitic beds were well indurated and behave as solid rafts in the megabreccia or as clasts in the tuffs, marly limestones were still soft, deformed ductilely in the megabreccia, and were injected in

Fig. 10. Syn-sedimentary deformation in the platy limestones, indicating sliding towards N190° to N220°. Same legend as for Fig. 9 for the stereo net; the thick great circle represents the sedimentary dike. Same notebook as for Fig. 7. Structural observations made in and around this outcrop are shown Fig. 3B in rose diagram (c). Location Figs. 3 and 4.

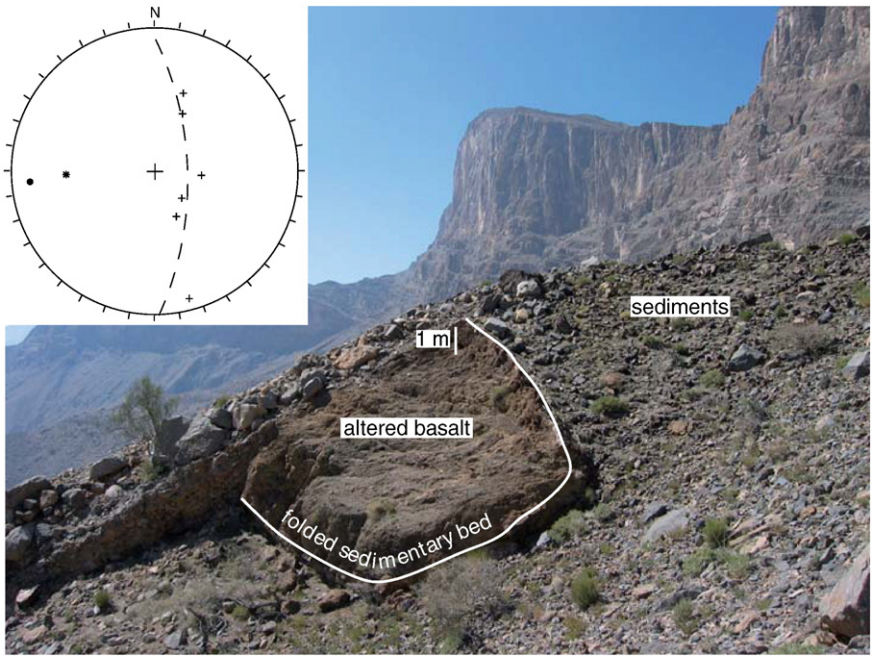

Fig. 11. Folded sedimentary bed within the lower magmatic stock (view towards WSW). Same legend for the stereo net as for Fig. 8; the black dot and the star represent the measured and computed fold axis, respectively. The fold axis is also shown Fig. 3B in rose diagram (j). Location Figs. 3 and 4.

tension gashes. Lime mud was probably the more recent sediment at sea-floor, and was incorporated in the eruption to form the matrix of the tuffs.

4.3. Evolution

It's possible to reconstruct in detail how the volcanic event proceeded (Fig. 13):

(1) During a first stage, the magma rose to the base of the lower limestones, probably along an incipient normal fault (Fig. 13-A). The magma intruded as sub-horizontal sills in the main sedimentary discontinuities, especially at the base of the lower limestones, which was probably the surface with the highest rheological contrast. Once the displacements induced by more recent faults have been removed, the present-day geometry indicates that this magmatic intrusion was saucer-shaped (Chevallier and Woodford, 1999), and less than 100 m below the sea-floor (Fig. 4). It was probably fed by a central magmatic body, as in the model proposed by Thomson and Hutton (2004). We call it a proto-magmatic body (Fig. 13A), as it represents an early stage of the upper magmatic stock. Although there is no direct evidence for it, it is assumed that the two magmatic bodies initiated at the same time. At this stage, there is no evidence of explosion associated with sill intrusion, suggesting the absence of an aquifer below the lower limestones.

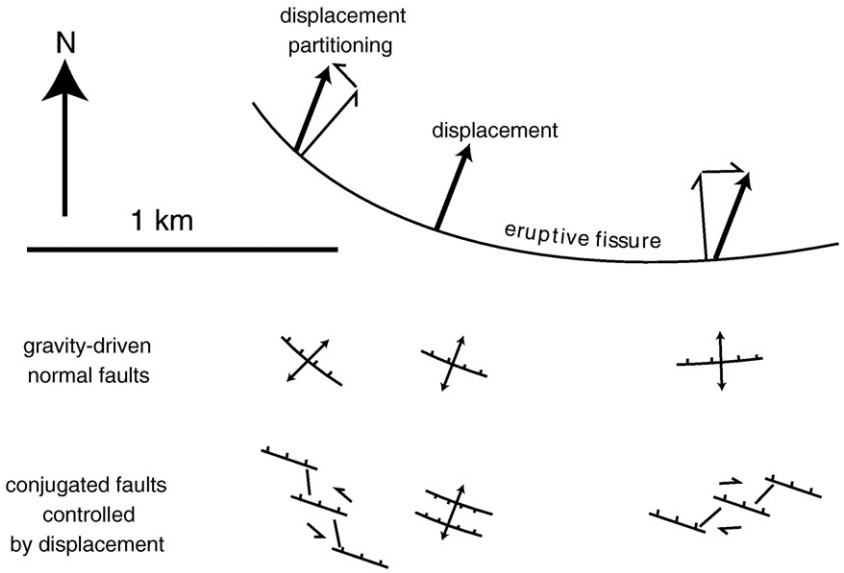

Fig. 12. Map view of the inferred eruptive fissure. Changes in fault strike are interpreted as an effect of displacement partitioning along an arcuate eruptive fissure. See text for comments.

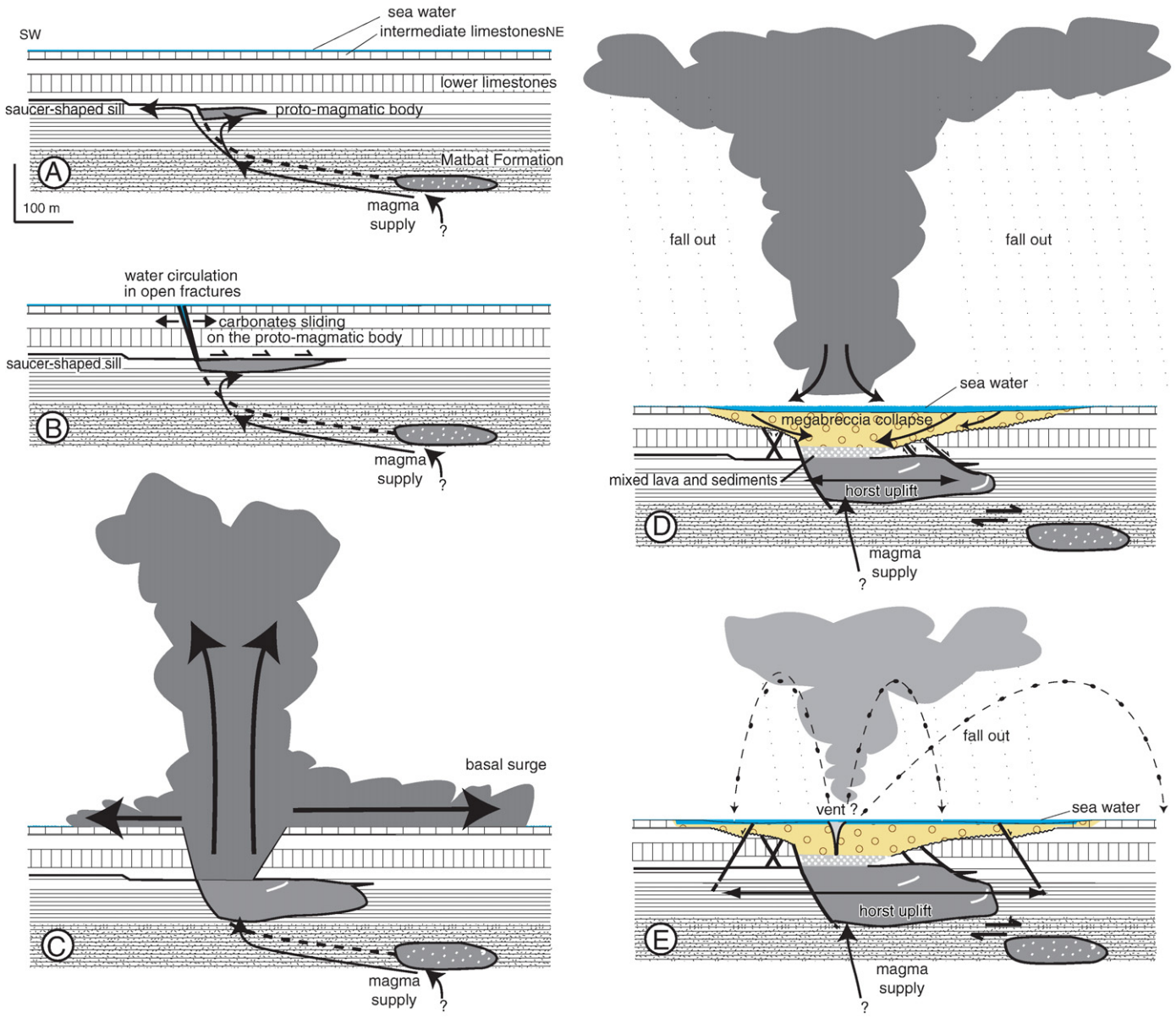

Fig. 13. Reconstitution of the successive stages of eruption. Stage E corresponds to Fig. 4. Dotted lines and question marks indicate inferred – but not observed – structures. See text for comments.

(2) The increasing size of the magmatic intrusion may have allowed the overlying carbonates to slide on the proto-magmatic body (Fig. 13-B). This destabilization may have opened tension cracks in the lower limestones, that brought sea water into contact with the magma. The resulting hydromagmatic explosion locally removed the overlying sediments on the normal fault hanging wall (Fig. 13-C). This eruption occurred in a marine environment, but displays sub-aerial attributes, indicating a very shallow sea, consistent with the carbonate platform environment (Pillevuit, 1993; Bernecker, 2007).

(3) At the surface, this explosion may have produced a crater, possibly elongated along a WNW–ESE direction similar to the underlying normal fault. The walls of the crater then collapsed, and the surface and subsurface sediments may have slid towards this crater, inducing in situ brecciation by breaking and sliding of the more lithified beds, mixed in a lime mud matrix (Fig. 13-D). This megabreccia lies on an erosional surface that represents the lower limit of the unstable sediments and that cross-cut the intermediate limestones, the lower tuffs, the upper part of the lower limestones, and the normal faults which are closest to the eruption center. The fact that the conjugated normal faults south of the vent do not cut the saucer-shaped sill suggests that they formed when the magma was still fluid in the sill, and consequently that the eruption was sub-contemporaneous with the intrusion.

(4) Back-stripping of the present-day section indicates that the sealed normal faults do not accommodate the subsidence of the northeast block, but instead the uplift of a narrow horst centered on the vent, contemporaneous with the eruption, but prior to the redeposition of the megabreccia. Normal faults farther from the center of the vent shift the bottom of the megabreccia, but are sealed at its top (Fig. 13-E). They define a wider horst formed during the stabilization of the megabreccia. The southernmost normal fault cuts the saucer-shaped sill, indicating that megabreccia stabilization was long enough to allow magma cooling and solidification in the sill. Enlarging horst formation can be understood as resulting from the inflation of the upper magmatic body, probably due to a very rapid magmatic ascent compensating the unloading produced by the explosion. The magmatic body clearly replaced the

enclosing limestones, with some remnants that sank and were deformed as blocks or layers in the magma.

(5) After the stabilization of the megabreccia, minor hydromagmatic explosions still produced ejecta, that fed the overlying tuffs and breccia. It indicates that the magma still locally met the sea water or soft sediments, probably in the mixed lava and sediment layer, located at the base of the vent between the magmatic body and the megabreccia. However, no eruptive structures such as vents or diatremes were observed across the megabreccia. These structures and the associated eruptions were probably smaller by several orders of magnitude than the initial one.

(6) During these first phases, the carbonate platform slid above ductile magma near the vent. Rapidly, the magma closest to the surface cooled and became solid, but the platform continued to slide northeastward on the underlying Matbat sediments and on the lower magma body that was cooling more slowly than the upper one (Fig. 13-E).

(7) Finally, the calcareous sedimentation proceeded again and sealed the whole structure. At that time the vent was probably a several meter-deep trough, where platy limestones were deposited. Differential compaction locally increased and maintained the subsidence along the vent (Lorenz, 2007), and explains the gravity-driven deformations that occurred during the platy limestones' deposition. Then the calcareous sedimentation proceeded homogeneously from the base of the upper limestones, with no significant lateral variations of facies nor thicknesses. Subsequent deformations and magmatic events deformed this structure later-on, as shown by the more recent N–S-striking dikes and veins cross-cutting the upper magmatic body (Chauvet, 2007).

5. Discussion

5.1. Comparison with the MIT guyot eruption

As stated in the Introduction, there is only one other published example of a volcanic eruption through an active carbonate platform, the MIT guyot (Shipboard Scientific Party, 1993; Martin et al., 2004). Both MIT guyot and Misfah platform present a tephra unit, that consists of a mix of palagonitized basaltic clasts and armoured lapilli in a carbonate mud. Both eruptions were hydromagmatic, triggered by the interaction between magma and water-saturated sediment in a semi-solidified carbonate platform. However, the tephra unit (MIT guyot) and upper tuff (Misfah) present significant differences: the tephra unit is 200 m-thick, with numerous sliding structures, while the upper tuffs are 10 meters-thick, and seal the deformed underlying megabreccia. One may propose that the Misfah's equivalent of the MIT guyot tephra unit can be the thick megabreccia, which has been also emplaced by gravity-driven sliding, and which contains few volcanic clasts. The difference between those two sites may be related to the rheology of the host sediments where the magma intruded. In the MIT guyot, a soft substrate may have been totally destabilized during the eruption, mixed with the magma, and subsequently displaced by grain flows and turbidity currents (Martin et al., 2004). In Misfah, the substrate has been rigidified by early diagenesis of carbonates, and especially of dolomites; this substrate slid after the initial explosion, but was too rigid to be significantly mixed with the magma during this explosion.

5.2. Eruptive behavior

Hydromagmatic eruptions occur in various environments, and result in various morphologies, structures and lithologies. This reflects eruptive behaviors mainly controlled by the local conditions that bring magma and water into contact. The vaporization of either phreatic or sea water in contact with the magma leads to violent explosions, to volcanic structures well-expressed in the topography (crater above a diatreme, tuff ring or scoria cone), and to characteristic volcanic formations or rock types (basal surge deposits, ejecta, hyaloclastites, palagonite). Is there a specific eruptive behavior associated with the carbonate platform sedimentary environment?

These platforms are below sea level and at shallow depth (a few meters to ten meters), but unlike Surtsey-type eruptions, no tuff- or scoria-cones were built during the eruption, because the lava did not reach the sea-floor and was not directly in contact with sea water. There are no lava flows and only a very restricted proportion of hyaloclastite or palagonite in the volcanic ejecta, while a significant magmatic volume was emplaced only few tens of meters below the sea-floor. The eruption seems to have been almost purely phreatic, with a very restricted proportion for the juvenile volcanic component of tephra, but there is no morphologic indication of a tuff ring that should have been well-recorded in a carbonate platform environment. There is no more sedimentary evidence of erosion and re-working of tuff materials, as should be expected for a tuff ring or cone leveled by wave action (Cas et al., 1989; Sohn et al., 2008).

Furthermore, there were no repeated phreatic eruptions at depth and no associated brecciated pipe, suggesting the sea water could not refill an aquifer in contact with the magma. This is probably related to the specific hydrology of carbonated platform, where both porosity and permeability are controlled partly by the changes of sedimentary facies, and mainly by the diagenetic evolution (Whitaker et al., 1997). After diagenesis, the carbonates behave as impermeable layers. Karstification during platform emersion and fracturation are the main processes that increase notably the carbonate permeability. In Misfah carbonate platform, fracturation of the shallower part of the platform may have been the initial mechanism that brought water in contact with a shallow-seated sill.

As in soft-substrate maar volcanoes (Auer et al., 2007), the widening and infilling of the vent were mainly the result of the collapse of the vent walls after an hydromagmatic eruption. However, as emphasized in the previous section, the collapse is controlled by the rheology of the sedimentary section. Soft sediments collapse and are mixed with magma during the eruptions, as in the example of the MIT guyot (Martin et al., 2004) or Jeju island unconsolidated sediments (Sohn and Park, 2005). In Misfah, early diagenesis allowed sedimentary beds or sets of beds to slide like rafts or tilted blocks within a muddy calcareous matrix to form a megabreccia. The displacements of these solid rafts may strongly control the evolution of the eruption, creating an impermeable lid that isolated the underlying magma from the overlying sea water, and consequently both the access of most of the magma to the surface, and the access of sea water to the magmatic stock. In this case, the eruptive behavior is first controlled by explosive processes (magma–water interaction) for the initial eruption, then by gravity-driven processes (destabilization of the sedimentary cover) that preclude any other significant eruption and the development of a diatreme. The interaction of the underlying magma with the water contained in the megabreccia (especially in the carbonate mud matrix) may have produced only small and secondary hydromagmatic explosions restricted to the mixed lava and sediment layer, at the top of the upper magmatic body.

5.3. Vent and diatreme shapes

When compared with continental maar-diatremes, the studied vent exhibits peculiar features. It has a broad and shallow bowl-shaped structure, similar in shape to the soft-substrate maar volcanoes, contrasting with the deep and steep-sided diatremes observed for hard-substrate maar volcanoes (Lorenz, 2003; Auer et al., 2007), including those that commonly occur in karst systems with carbonated rocks (Nemeth et al., 2001). While most limestones and dolomitic layers were solidified by early diagenesis by the time of

eruption, the mechanical behavior (slope failure and angle of repose: Barnet, 2008) of the host rocks depended on the proportion and mixing of soft layers (marls, lime mud) and hard layers (limestones, dolostones) in the affected sedimentary section. The resulting collapse of the sides of the vent at the time of eruption appears mainly controlled by the soft layers.

The second process that significantly controls the shape of a maar-diatreme volcano is the depth of initial interaction between magma and water, and the repetition of this interaction at deeper levels in the diatreme, inducing the downward penetration of the explosion locus and the steepening of the cone-shaped diatreme (Lorenz, 1986). As proposed in other settings (Houghton et al., 1999; Nemeth and Martin, 2007), the initial water/magma interaction occurred at a shallow depth, less than 100 m. In the studied case water refilling may be favored by a subaquatic setting, but appears to have been prevented by the lack of permeability of the megabreccia filling the diatreme.

5.4. Volcanism–sedimentation interaction

The initial hydromagmatic explosion locally removed the topmost formations. It induced a pressure fall at depth (Lorenz, 1974; Lorenz and Kurszlaukis, 2007), that allowed the ascent of a significant volume of magma and its emplacement below the lower limestones. This magma represented a decollement layer, where the limestones could slide away from the vent. Sliding increased the unloading, allowing more magma to be emplaced at shallow depth. Rising magma produced a tectonic instability, that in return favoured the magma ascent in a feedback mechanism. Comparable feedback has been proposed for the emplacement of magmatic domes such as Mt St. Helens (Lipman and Mullineaux, 1981). In this pelean eruption, the emplacement of a crypto-dome at depth triggered a tectonic instability (gravitational sliding on the volcano flanks), that induced the blast by decompression of the unroofed crypto-dome.

The eruption induced very limited changes in the carbonate sedimentation. At the time of the eruption, carbonate sedimentation probably locally ceased because of water turbidity, and only previously formed sediments were reworked. One may expect vertical displacements and carbonate facies changes associated with the volcanic event, but they appear to be restricted. The subsurface intrusions are mainly compensated by the removal of the overlying sediments, either by their projection during the eruption or by sliding in the megabreccia. Local uplift above the vent can be estimated from the slip on normal faults: it represents no more than 20% of the observed thickness of the upper magmatic stock, and this vertical displacement is almost totally absorbed within the megabreccia. The only significant effect on sedimentation is a local increase of depth and subsidence in the vent area (Lorenz, 2007), allowing deposition of platy limestones. This change does not seem to be strictly related to the eruption, but mainly to the compaction of the megabreccia that filled the vent.

6. Conclusion

We presented a detailed description of a hydromagmatic eruption both within, and coeval with, an active carbonate platform. While this eruption occurred below sea level, we did not observe tuff- or scoria-cones at surface nor brecciated pipe underground, that may have indicated a repeated contact between magma and sea water. We found two superposed magmatic bodies that intruded the sedimentary cover a few tens of meters below the sea-floor. At the top of the shallower magmatic stock, the sediments were locally removed by a hydromagmatic eruption, and the host sediments collapsed from the walls of the vent to form a megabreccia. The megabreccia filled the vent and prevented any further contact between sea water and magma. This allowed the inflation of a shallower magmatic body, with at its top, a 20 meters-thick layer where magma and sediments have been mixed together. The small quantity of water available in the sediment allowed only small explosions from this mixed layer. This volcanic structure is quite similar to sub-aerial maars erupted in soft sediments. It underlines that the main control factor on hydromagmatic eruptions is not the amount of available water, but the mechanisms that bring into contact water and magma. In the studied case the rheology of lime mud and limestones appears to be a key parameter, and was probably mainly controlled by early diagenesis.

Structural observations from the sedimentary section and the syn-volcanic deposits suggest that the eruption did not produce a circular vent, but an arcuate fissure, probably related to the gravity-driven sliding of the carbonate platform towards its edge. We also suggest that these gravity-driven displacements may be an important control factor in the eruptive behavior, as they localized the rising of magma and prevented repeated hydromagmatic explosions.

Finally, it is important to note that a very small amount of the magmatic rocks reached the surface during this eruption, and that it may induce an underestimation of this type of volcanism coeval with the building of carbonate platforms.

Acknowledgements

This paper is dedicated to our colleague Henriette Lapierre, deceased in January 2006, who initiated our work in Oman. The field work has been partially funded by the Groupement de Recherche 'Marges'. The Centre National de Recherche Scientifique and Université Joseph Fourier also provided financial support, together with various funds initially scheduled for other scientific works. We thank F. Béchennec and N. Arndt for very fruitful discussions at various stages of this work, and Dr Hilal Mohammed Sultan Al Azri from the Omani Ministry of Commerce and Industry for his kind welcome and support in Oman. Rose diagrams and stereo nets were drawn using A. Pecher's Stem software. The manuscript benefited from thorough reviews by K. Nemeth and an anonymous reviewer, and was kindly checked by A. Bargery. By reference to the goats grazing in the magmatic stock, we shall appreciate if this volcanic event and the associated structures will be named Goat's Volcano.

References

Auer, A., Martin, U., Németh, K., 2007. The Fekete-hegy (Balaton Highland Hungary) "soft-substrate" and "hard-substrate" maar volcanoes in an aligned volcanic complex – implications for vent geometry, subsurface stratigraphy and the palaeoenvironmental setting. J. Volcanol. Geotherm. Res. 159, 225–245.

Barnet, W.P., 2008. The rock mechanics of kimberlite volcanic pipe excavation. J. Volcanol. Geotherm. Res. 174, 29–39.

Baud, A., Béchennec, F., Cordey, F., Krystyn, L., Le Métour, J., Marcoux, J., Maury, R., Richoz, S., 2001. Permo-Triassic deposits: from the platform to the basin and seamounts. International Conference on the Geology of Oman, Excursion n°A01. 56 pp.

Béchennec, F., 1988. Géologie des nappes Hawasina dans les parties orientales et centrales des montagnes d'Oman. Doc, vol. 127. BRGM. 474 pp.

Béchennec, F., Le Métour, J., Rabu, D., Villey, M., Beurrier, M., 1988. The Hawasina Basin: a fragment of a starved passive continental margin, thrust over the Arabian Platform during obduction of the Sumail Nappe. Tectonophysics 151, 323–343.

Béchennec, F., Le Métour, J., Rabu, D., Bourdillon-Jeudy de Grissac, C., De Wever, P., Beurrier, M., Villey, M., 1990. The Hawasina Nappes: stratigraphy, paleogeography, and structural evolution of a fragment of the south-Tethyan passive continental margin. In: Robertson, A.H.F., et al. (Ed.), The Geology and Tectonics of the Oman Region. Spec. Public., vol. 49. Geol. Soc., pp. 213–224.

Béchennec, F., Tegyey, M., Le Métour, J., Lemière, B., Lescuyer, J.L., Rabu, D., Milesi, J.P., 1991. Igneous rocks in the Hawasina Nappes and the Al-Hajar supergroup, Oman mountains: their significance in the birth and evolution of the composite extensional margin of eastern Tethys. In: Peters, T., et al. (Ed.), Ophiolite genesis and evolution of the oceanic lithosphere. Kluwer Academy, Norwell, Massachusetts, pp. 569–611.

Beltramo, J., 2003. Les séries carbonatées crétacées d'arc volcanique du Terrane Guerrero (Mexique). Ph. D. Thesis, Univ. Joseph Fourier, Grenoble, France, 296 pp.

Bernecker, M., 2007. Facies architecture of an isolated carbonate platform in the Hawasina Basin: the Late Triassic Jebel Kawr of Oman. Pal. Pal. Pal. 252, 270–280.

Beurrier, M., Béchennec, F., Rabu, D., Hutin, G., 1986. Geological map of Rustaq: sheet NF40-3A, Scale 1/100 000. Sultanate of Oman, Ministry of Petroleum and Minerals, Directorate General of Minerals. BRGM, Orléans. Editor.

Blendinger, W., 1985. Middle Triassic strike-slip tectonics and igneous activity of the Dolomites (Southern Alps). Tectonophysics 113, 105–121.

Buigues, D., Gachon, A., Guille, G., 1992. L'atoll de Mururoa (Polynésie française) I. – Structure et évolution géologique. Bull. Soc. Géol. France 163, 645–657.
Cas, R.A.F., Landis, C.A., Fordyce, R.E., 1989. A monogenetic, Surtla-type, Surtseyan volcano from the Eocene–Oligocene Waiareka-Deborah volcanis, Otago, New Zealand: a model. Bull. Volcanol. 51, 281–298.
Chauvet, F., 2007. La marge continentale sud-téthysienne en Oman: structure et volcanisme au Permien et au Trias. Ph. D. Thesis, Univ. Joseph Fourier, Grenoble, France, 420 pp.
Chevallier, L., Woodford, A., 1999. Morpho-tectonics and mechanism of emplacement of the dolerite rings and sills of the western Karoo, South Africa. S. Afric. J. Geol. 102, 43–54.
Cole, P.D., Guest, J.E., Duncan, A.M., Pacheco, J.M., 2001. Capelinhos 1957–1958, Faial, Azores: deposits formed by an emergent surtseyan eruption. Bull. Volcanol. 63, 204–220.
Fernández-Mendiola, P.A., García-Mondéjar, J., 2003. Carbonate platform growth influenced by contemporaneous basaltic intrusion (Albian of Larrano, Spain). Sedimentology 50, 961–978.
Fisher, R.V., 1977. Erosion by volcanic base-surge density currents: U-shaped channels. Geol. Soc. Am. Bull. 88, 1287–1297.
Fulthorpe, C.S., Schlanger, S.O., 1989. Paleo-oceanographic and tectonic settings of Early Miocene reefs and associated carbonates of offshore Southeast Asia. Am. Assoc. Petrol. Geol. Bull. 73, 729–756.
Gençalioglu-Kuscu, G., Attila, C., Cas, R.A.F., Kuscu, I., 2007. Base surge deposits, eruption history, and depositional processes of a wet phreatomagmatic volcano in Central Anatolia (Cora Maar). J. Volcanol. Geotherm. Res. 159, 198–209.
Glennie, K.W., Bœuf, M.G.A., Hughes Clarke, M.W., Moody-Stuart, M., Pillaart, W.F.H., Reinhart, B.M., 1973. Late Cretaceous nappes in the Oman mountains and their geologic significance. Am. Assoc. Petrol. Geol. Bull. 57, 5–27.
Glennie, K.W., Bœuf, M.G.A., Hughes Clarke, M.W., Moody-Stuart, M., Pillaart, W.F.H., Reinhart, B.M., 1974. Geology of the Oman mountains. Geol. Mijnb. 1 423 pp.
Graham, G.M., 1980. Structure and sedimentation of the Hawasina window, Oman mountains. Ph. D. Thesis. Milton Keynes, England, Open University, 422 pp.
Hess, H.H., 1946. Drowned ancient islands of the Pacific basin. Am. J. Sci. 244, 772–791.
Houghton, B.F., Wilson, C.J.N., Smith, I.E.M., 1999. Shallow-seated controls on styles of explosive basaltic volcanism: a case study from New Zealand. J. Volcanol. Geotherm. Res. 91, 97–120.
Kokelaar, B.P., 1983. The mechanism of Surtseyan volcanism. J. Geol. Soc. London 140, 939–944.
Lipman, P.W., Mullineaux, D.R. (Eds.), 1981. The 1980 Eruptions of Mount St. Helens. Profess. Pap., vol. 1250. US Geol. Surv. 844 pp.
Lorenz, V., 1974. On the formation of maars. Bull. Volcanol. 37, 183–204.
Lorenz, V., 1986. On the growth of maars and diatremes and its relevance to the formation of tuff rings. Bull. Volcanol. 48, 265–274.
Lorenz, V., 2003. Maar-diatreme volcanoes, their formation, and their setting in hard-rock and soft-rock environments. Geolines 15, 72–83.
Lorenz, V., 2007. Syn- and posteruptive hazards of maar-diatreme volcanoes. J. Volcanol. Geotherm. Res. 159, 285–312.
Lorenz, V., Kurszlaukis, S., 2007. Root zone processes in the phreatomagmatic pipe emplacement model and consequences for the evolution of maar-diatreme volcanoes. J. Volcanol. Geotherm. Res. 159, 4–32.
Machado, F., Richards, A.F., Mulford, J.W., Parsons, W.H., 1962. Capelinhos eruption of Fayal volcano, Azores, 1957–1958. J. Geophys. Res. 67, 3519.
Martin, U., Nemeth, K., 2005. Eruptive and depositional history of a Pliocene tuff ring that developed in a fluvio-lacustrine basin: Kissomlyo volcano (Western Hungary). J. Volcanol. Geotherm. Res. 147, 342–356.
Martin, U., Breitkreuz, C., Egenhoff, S., Enos, P., Jansa, L., 2004. Shallow-marine phreatomagmatic eruptions through a semi-solidified carbonate platform (ODP Leg 144, Site 878, Early Cretaceous, MIT Guyot, West Pacific). Mar. Geol. 204, 251–272.
Matthews, J.L., Heezen, B.C., Catalano, R., Coogan, A., Tharp, M., Natland, J., Rawson, M., 1974. Cretaceous drowning of reefs on Mid-Pacific and Japanese guyots. Science 184, 462–464.
Nemeth, K., Martin, U., 2007. Shallow sill and dyke complex in western Hungary as a possible feeding system of phreatomagmatic volcanoes in "soft-rock" environment. J. Volcanol. Geotherm. Res. 159, 138–152.
Nemeth, K., Martin, U., Harangi, S., 2001. Miocene phreatomagmatic volcanism at Tihany (Pannonian Basin, Hungary). J. Volcanol. Geotherm. Res. 111, 111–135.
Pardo, N., Avellan, D.R., Macias, J.L., Scolamacchia, T., Rodriguez, D., 2008. The ~1245 yr BP Asososca maar: new advances on recent volcanic stratigraphy of Managua (Nicaragua) and hazard implications. J. Volcanol. Geotherm. Res. 176, 493–512.
Pillevuit, A., 1993. Les blocs exotiques du sultanat d'Oman, évolution paléogéographique d'une marge passive flexurale. Ph. D. thesis, Mém. Géol., Lausanne, 17, 249 pp.
Pillevuit, A., Marcoux, J., Stampfli, G., Baud, A., 1997. The Oman exotics: a key to the understanding of the Neotethyan geodynamic evolution. Geodin. Acta 10, 209–238.
Robertson, A.H.F., Searle, M.P., 1990. The northern Oman Tethyan continental margin: stratigraphy, structure, concepts, and controversies. In: Robertson, A.H.F., et al. (Ed.), The Geology and Tectonics of the Oman Region. Spec. Public., vol. 49. Geol. Soc., pp. 3–25.
Searle, M.P., Graham, G.M., 1982. "Oman exotics" – oceanic carbonate build-ups associated with the early stage of continental rifting. Geology 10, 43–49.
Sengör, A.M.C., Cin, A., Rowley, D.B., Nie, S.Y., 1993. Space-time patterns of magmatism along the Tethysides: a preliminary study. J. Geol. 101, 51–84.
Sheridan, M.F., Wohletz, K.H., 1983. Hydrovolcanism: basic considerations and review. J. Volcanol. Geotherm. Res. 17, 1–29.
Shipboard Scientific Party, 1993. Site 878. In: Premoli Silva, I., Haggerty, J., Rack, F., et al. (Eds.), Proceedings ODP. Init. Rep., vol. 144. Ocean Drilling Program, College Station, TX, pp. 331–412.
Sohn, Y.K., Park, K.H., 2005. Composite tuff ring/cone complexes in Jeju Island, Korea: possible consequences of substrate collapse and vent migration. J. Volcanol. Geotherm. Res. 141, 157–175.
Sohn, Y.K., Park, K.H., Yoon, S.H., 2008. Primary versus secondary and subaerial versus submarine hydrovolcanic deposits in the subsurface of Jeju Island, Korea. Sedimentology 55, 899–924.
Soja, C.M., 1996. Island-arc carbonates; characterization and recognition in the ancient geologic record. Earth Sci. Rev. 41, 31–65.
Solgevik, H., Mattsson, H.B., Hermelin, O., 2007. Growth of an emergent tuff cone: fragmentation and depositional processes recorded in the Capelas tuff cone, São Miguel, Azores. J. Volcanol. Geotherm. Res. 159, 246–266.
Stampfli, G., Marcoux, J., Baud, A., 1991. Tethyan margins in space and time. Palaeogeo. Palaeoclim. Palaeoeco. 87, 373–409.
Thomson, K., Hutton, D., 2004. Geometry and growth of sill complexes: insights using 3D seismic from the North Rockall Trough. Bull. Volcanol. 66, 364–375.
Thorarinsson, S., 1967. Surtsey. The New Island in the North Atlantic. Viking, New York. 68 pp.
Whitaker, F., Smart, P., Hague, Y., Waltham, D., Bosence, D., 1997. Coupled two-dimensional diagenetic and sedimentological modeling of carbonate platform evolution. Geology 21, 175–178.
White, J.D.L., 1991. Maar-diatreme phreatomagmatism at Hopi Buttes, Navajo Nation (Arizona, USA). Bull. Volcanol. 53, 239–258.
White, J.D.L., 1996. Impure coolants and interaction dynamics of phreatomagmatic eruptions. J. Volcanol. Geotherm. Res. 74, 155–170.
Wohletz, K., 1986. Explosive magma–water interactions: thermodynamics, explosion mechanisms, and field studies. Bull. Volcanol. 48, 245–264.
Zimanowski, B., Frohlich, G., Lorenz, V., 1991. Quantitative experiments on phreatomagmatic explosions. J. Volcanol. Geotherm. Res. 48, 341–358.